

## ARTICLE

## Surface indentation and fluid intake generated by the polymer matrix of *Bacillus subtilis* biofilms

Cite this: DOI: 10.1039/x0xx00000x

W. Zhang,<sup>a</sup> W. Dai,<sup>b</sup> Shi-Ming Tsai,<sup>c</sup> S.M. Zehnder,<sup>b</sup> M. Sartinoranont,<sup>b,d,e</sup> and T. E. Angelini<sup>b,d,e</sup>Received 00th January 2012,  
Accepted 00th January 2012

DOI: 10.1039/x0xx00000x

[www.rsc.org/](http://www.rsc.org/)

Bacterial biofilms are highly structured, surface associated bacteria colonies held together by a cell-generated polymer network known as EPS (extracellular polymeric substance). This polymer network assists in adhesion to surfaces and generates spreading forces as colonies grow over time. In the laboratory and in nature, biofilms often grow at the interface between air and an elastic, semi-permeable nutrient source. As this type of biofilm increases in volume, an accommodating compression of its substrate may arise, potentially driven by the osmotic pressure exerted by the EPS against the substrate surface. Here we study *Bacillus subtilis* biofilm force generation by measuring the magnitude and rate of deformation imposed by colonies against the agar-nutrient slabs on which they grow. We find that the elastic stress stored in deformed agar is orders of magnitude larger than the drag stress associated with pulling fluid through the agar matrix. The stress exerted by the biofilm is nearly the same as the osmotic pressure generated by the EPS, and mutant colonies incapable of producing EPS exert much lower levels of stress. The fluid flow rate into *B. subtilis* biofilms suggest that EPS generated pressure provides some metabolic benefit as colonies expand in volume. These results reveal that long-term biofouling and colony expansion may be tied to the hydraulic permeability and elasticity of the surfaces that biofilms colonize.

### Introduction

Bacterial biofilms are a class of physically robust and chemically resistant bacteria colonies responsible for tissue and medical implant infection<sup>1-3</sup>, tooth decay<sup>4,5</sup>, and the general fouling of surfaces in nature and industry<sup>6</sup>. Biofilms produce several types of polymer that provide the colony with surface adhesion, elasticity, and strength<sup>7-11</sup>. This matrix of polymers, known as extracellular polymeric substance (EPS), constitutes 75-90% of the biofilm by volume<sup>6,12</sup>, and a major component of the EPS is polysaccharide<sup>9,13-15</sup>. The polysaccharides are long, flexible, and strongly solvated by water, enabling them to generate osmotic pressure<sup>16</sup>. Polysaccharide generated osmotic pressure can drive fluid flow throughout a biofilm, producing forces that spread the colony across its substrate<sup>17</sup>. EPS production in biofilms is nonlinear in time; production is slow when the colony is small and increases dramatically when the colony becomes large. When this increase in EPS production occurs, the colony expands radially, further increasing biofilm volume. This increase in EPS production also occurs when the colony hits a diffusion-limited nutrient transport bottleneck<sup>18</sup>.

In the laboratory, biofilms are typically grown submerged in fluid flow cells, as pellicles at air-water interfaces, or as colonies on permeable agar substrates<sup>19</sup>. For biofilms grown on agar, nutrients and water transfer from the hydrogel substrate into the colony. The

mechanical compression of the biofilm's substrate during this process, possibly driven by EPS generated osmotic pressure, has not been explored. A broader understanding of surface biofouling and new strategies to prevent colony expansion may be possible if mass transport into biofilms is tied to the hydraulic permeability and elasticity of the substrates containing their nutrient sources, as in infected tissue, for example.

Here we investigate the stresses *Bacillus subtilis* biofilms exert on their substrates. We grow biofilms on large agar slabs and on top of narrow agar cylinders, observing the magnitude and rate of substrate compression. We find that the colonies indent their agar substrates most dramatically when EPS production increases, and that EPS knockout mutants indent their substrates very little. We measure the stress exerted on the substrate surface by the biofilm, and we find that elastic stress is much larger than the viscous stress associated with fluid drag; elastic stresses stored in the deformed agar reach hundreds of Pascals, yet fluid stresses only reach a few Pa. We compare our measurements to a finite element model of substrate indentation by the biofilm, showing that biofilm-generated stresses are dominantly normal to the surface. From measurements of fluid flow out of the agar substrate into the biofilm, we estimate a Péclet number of 0.7, demonstrating that the EPS driven compression of the substrate enhances diffusive nutrient transport compared to diffusion alone.

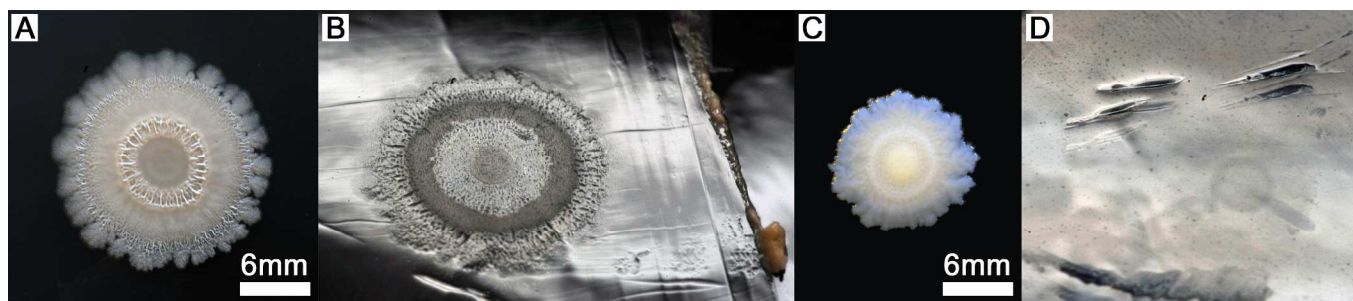


**Figure 1.** Substrate indentation is routinely observed with *Bacillus subtilis* biofilms grown on agar. A *B. subtilis* biofilm exhibits a rough, wrinkly surface (A), and an indent below the biofilm is revealed by gently scraping the colony from the agar (B). A mutant colony that does not produce polysaccharide appears smooth and shiny at its surface (C) and does not produce a visible indent in the agar substrate (D).

## Results

**Biofilm Colonies Indent Their Substrate.** To explore biofilm generated forces on permeable elastic substrates, we grow *B. subtilis* colonies following established laboratory protocols<sup>20</sup>. 5  $\mu$ l of *B. subtilis* strain NCIB3610 from shaking culture is spotted onto 1.5% agar plates saturated with minimal salts glycerol glutamate (MSgg) medium. The culture plates are inverted and incubated at 37°C and 95% humidity. After 12–24 hours of incubation, the colony attains a rough appearance associated with an increased production of EPS<sup>21</sup>. When the colony is gently scraped from the agar, a small indentation is observed in the region where the biofilm previously sat. We perform the same tests on colonies grown for longer periods of time, and find that the indent increases in width and visible topographical roughness as the colony spreads. When the same qualitative tests are performed on a mutant strain that does not produce polysaccharide (EPS<sup>-</sup>), the colony remains smooth and no indent is visible (Fig. 1). Other researchers have reported this phenomenon to us in conversation, and we routinely observe this behavior in *B. subtilis* biofilms when performing assays that require harvesting the colony<sup>21</sup>. To test whether the indent is reversible, we submerge the entire colony in water after the colony is removed. We find that the indented agar swells, recovering from the indentation in less than an hour. The same results are achieved regardless of whether the colony is grown on top of the agar or below the agar on an inverted petri dish.

**Microscopic Pressure Measurements.** To measure the depth of biofilm indentation into agar throughout space and time, we monitor colonies on an inverted microscope in an environmentally controlled chamber kept at 37°C and saturated humidity. We dope the agar-MSgg substrate with 1  $\mu$ m diameter fluorescent microspheres and collect z-stacks of fluorescence images in time-lapse at 14 lateral positions, spanning

approximately two centimeters across the petri-dish. The agar slab is approximately 3mm thick, so a long-working distance 4x objective with a low numerical aperture is used to collect images. The low numerical aperture precludes high-resolution z-sectioning, so z-slices are spaced by a distance of 11  $\mu$ m. At each lateral location, the highest plane in which beads are in focus determines the vertical location of the agar-biofilm interface. These locations are used to construct a map of the interface at each 45 minute delay interval over a 22.5-hour period (Fig. 2A,B).

We find that the wild-type (WT) biofilm begins to indent the agar after about 4 hours, and indents approximately 45  $\mu$ m into the substrate by 16.5 hours. By contrast, the EPS<sup>-</sup> strain exhibits a measureable indent after around 13 hours, and only indents approximately 15  $\mu$ m into the agar after 16.5 hours. The deeper indent made by the WT strain compared to the EPS<sup>-</sup> strain demonstrates the role the EPS plays in generating pressure. To estimate the total volume indented, we fit the indentation profiles with a Gaussian curve and, assuming azimuthal symmetry, we compute the volume of the corresponding 2D Gaussian surface. The WT colony intends reach a maximum volume of 0.7 mm<sup>3</sup> while the EPS<sup>-</sup> colonies only indent up to 0.1 mm<sup>3</sup> (Fig. 2 C). The change in volume over time of the WT colony coincides with the increase of EPS production, previously observed in the same system<sup>18</sup>.

The millimeter-scale lateral footprint of the biofilm combined with the micrometer-scale indentation depth generates a depression with extremely low curvature, suggesting that the elastic strain and stress in the indented agar will dominantly arise in the z-direction. Additionally, we see no significant in-plane strain over long lengthscales in the

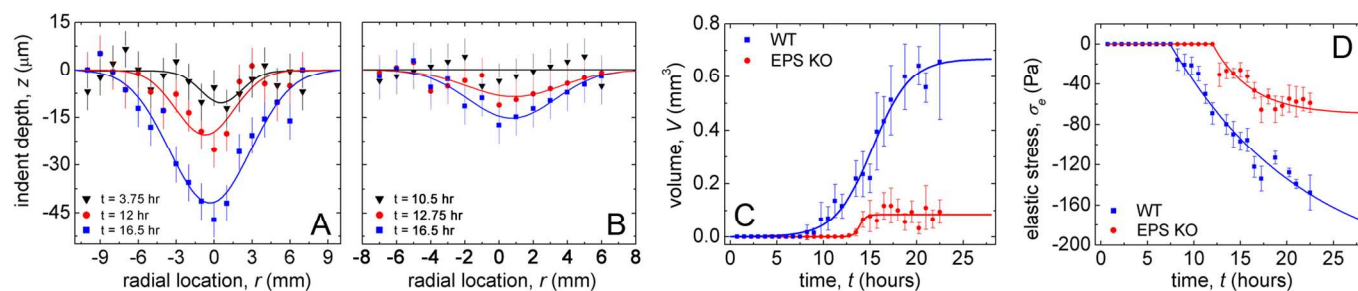


**Figure 2.** Biofilm generated indentation into agar substrates is measured with time-lapse microscopy, collecting z-stacks at multiple lateral locations, spanning 2cm. The WT biofilm generates large indents (A), and EPS<sup>-</sup> mutants indent the agar substrate much less (B). Fitting the indentation profiles with Gaussian lineshapes, we estimate the total indentation volume over time (C). Assuming a bed-of-springs model we compute the average stress exerted at the surface by the biofilm (D).

fluorescence images, though at higher magnification local deformations are likely to occur. We therefore approximate the agar as a bed of springs, and compute the stress in each volume element to be  $\sigma_e = E\delta h/h$ , where  $\delta h$  is the local indentation depth determined by the Gaussian fits,  $h$  is the un-deformed thickness of the agar slab, and  $E = 23$  kPa is the agar Young's modulus. The Young's modulus was measured in compression tests in a parallel plate rheometer with unconstrained circumferential boundaries at low strains (up to 2%) and low strain rates ( $1\% \text{ s}^{-1}$ ). We calculate the mean stress by averaging over the indented volume, which spans lengthscales much larger than the sub-micron heterogeneities in agar<sup>22</sup>. These geometric assumptions are tested with finite element calculations, below. This simplified model of biofilm indentation shows the stress generated by the WT colony growing steadily over time, reaching 150 Pa at the final time-point; the EPS<sup>-</sup> colony plateaus early at about 50 Pa, highlighting the major contribution of polysaccharide to stress generation (Fig 2D).

**Biofilm Growth and Force Generation in 1D.** To measure the stresses from fluid drag as flow is driven through the agar into the biofilm, in addition to measuring the elastic stresses with a second method, we perform an experiment in which the biofilm expansion occurs along a single direction. The biofilm is confined to a fixed diameter by a glass cylinder with a radius of 3.3 mm, growing on a column of agar with a height of 27.2 mm, also inside the glass cylinder. Images are taken from the side of the agar-biofilm interface to monitor the motion of the interface over time. The colony is incubated at  $37^\circ \text{ C}$  and photographed with a digital camera at 3-minute intervals over a period of 30 hours. The experiment is repeated with the EPS-mutant, and with an additional control experiment with no bacteria (Fig. 3A).

We generate a kymograph of WT colony growth by averaging each image in the lateral direction, and splicing the resulting intensity maps together in chronological order. The biofilm-agar interface appears as a high-contrast band of low-intensity pixels, which produce a bright peak in the kymographs when the intensity levels are inverted. The location of the interface at each time point is obtained by fitting a Gaussian curve along the vertical axis of the kymograph at each time point; the location of the interface is determined from the peak position of the Gaussian fit. The WT colony begins to rapidly indent the agar after 4 hours of growth at a rate of  $\sim 20 \mu\text{m hr}^{-1}$  until hour 15, consistent with the timing of EPS production<sup>18</sup>. From control experiments in which no bacteria are seeded onto the agar, we find that a small amount of evaporation drives the agar surface downward at a rate of  $2 \mu\text{m hr}^{-1}$ . The interface of the EPS<sup>-</sup> strain and agar moves a rate slightly larger than the rate of evaporation in the control experiment. The effects of water evaporation on transport within the biofilm have been explored previously<sup>19</sup>. We compensate for the effects of evaporation to isolate the effects of biofilm generated pressure by subtracting the control curve from the colony data. We find that the WT strain ultimately indents the agar by  $180 \mu\text{m}$ , while the EPS<sup>-</sup> mutant indents by only  $20 \mu\text{m}$  (Fig. 3B-D).

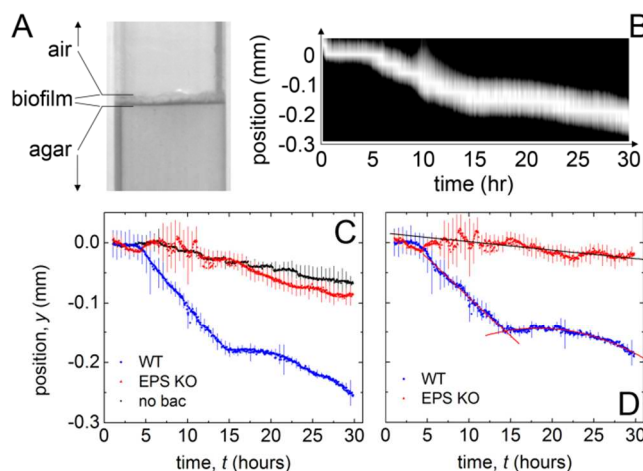


**Figure 3.** To simplify measurements of elastic stress and fluid flow into the biofilm as it expands, we confine the colony to glass tube of 3.3 mm radius. The biofilm-agar interface appears as a flat, high-contrast band (A) which we follow in time by constructing a kymograph (B). By fitting the peak in the kymograph over time, we identify the biofilm-agar interface to sub-pixel accuracy, finding that the WT biofilm deforms the agar much more than the EPS<sup>-</sup> mutant (C). Correcting for evaporation effects, the agar deformation curves are fit with polynomials to determine deformation rates (D).

**Comparison between fluid stress and elastic stress in 1D.** To determine the rate of indentation,  $dh/dt$ , and to calculate the volumetric flow rate over time, low-order polynomials are fit to the biofilm-agar interface locations. The drag stress associated with driving fluid through the column of agar along its length is  $\sigma_f = -k^{-1}A^{-1}LQ$ , where  $k$  is the agar permeability,  $A$  is the agar cross-sectional area,  $L$  is the length of the column, and  $Q$  is the volumetric flow rate. We measure  $Q$  throughout our experiments by computing  $A dh/dt$ , and we determine  $k = 2.6 \times 10^{-11} \text{ m}^2 \text{ Pa}^{-1} \text{ s}^{-1}$  in independent flow tests. We find that  $\sigma_f$  is very small throughout biofilm growth, reaching about 4 Pa at times of fastest indentation in the WT colonies and maintaining a constant value of about 0.5 Pa in the EPS<sup>-</sup> colonies (Fig. 4A).

With the confined 1D geometry in which the total hydrogel volume is forced to compress, the elastic stress is  $\sigma_e = K \delta h/h$ , where  $K$  is the bulk modulus,  $\delta h$  is the indentation depth, and  $h$  is the length of the agar column. To compute  $\sigma_e$ , we use the Young's modulus,  $E = 23$  kPa, in place of the bulk modulus because agar has a Poisson's ratio,  $\nu$ , of about  $1/3$ <sup>23</sup>. In the WT colonies, the stress rises linearly from 0 Pa to 125 Pa between 5 and 15 hours of growth, reaching 150

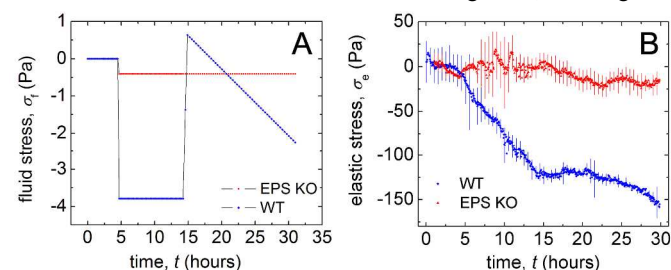


**Figure 4.** From the speed of the biofilm-agar interface, the fluid flow rate is computed and fluid drag stresses are estimated using Darcy's law. The fluid stresses are much larger for the WT biofilm than for the EPS<sup>-</sup> mutant due to the rapid expansion period of the WT strain (A). From the modulus and the linear strain of the agar cylinder, we compute the elastic stress generated by the biofilms, finding that elastic stresses are much larger than fluid drag stresses, and that the WT colony generates much larger stresses than the EPS<sup>-</sup> mutant (D).

Pa at 30 hours. In the EPS colony, by contrast, the stress begins to rise after about 15 hours and reaches about 25 Pa at 30 hours. Thus, the overall stress levels and progression of elastic stress in time are similar to those observed in colonies grown on plates. Moreover, the elastic stresses in the agar are always about two orders of magnitude larger than the fluid drag stresses, demonstrating that the stress generated by the biofilm can be inferred from the elastic stresses applied to the agar surface (Fig. 4 B).

**Finite Element Modelling of Elastic Stress.** In our analyses of biofilm growth in petri dishes and confined tubes, we have made the simplifying assumption that stresses are exerted primarily in the vertical direction. This is a good approximation in the 1D confined geometry, evidenced by the flat bottom of the biofilm, but the approximation may break down in petri dishes where the biofilm-agar interface is curved. To explore the potential generation of shear and horizontal stresses by biofilms grown unconfined on broad surfaces, we input the measured indentation profiles into a finite element analysis (FEA) simulation, measuring the resulting vertical stress,  $\sigma_{zz}$ , shear stress,  $\sigma_{rz}$ , and horizontal stress,  $\sigma_{rr}$ . In the FEA simulation, a 2D axi-symmetric geometry corresponding to the agar slab with a radius of 32.5 mm and height of 2.9 mm is generated. Agar is assumed to behave as a linear elastic material ( $E=23$  kPa,  $\nu=0.35$ ). The best-fit Gaussian shape profiles, described above, are input as the displacement boundary condition of the top surface to predict stresses throughout the agar volume. Fixed boundary conditions are assumed along other wall boundaries. The model consists of 900 8-node rectangular elements and is solved using the software package ADINA (v.8.5.0, Watertown, MA).

Stress maps in the  $r$ - $z$  plane show that vertical stresses,  $\sigma_{zz}$ , are dominant while in-plane stresses,  $\sigma_{rr}$ , are much smaller. Shear stresses,  $\sigma_{rz}$ , are roughly three orders of magnitude smaller than both  $\sigma_{zz}$  and  $\sigma_{rr}$ . Iso-stress contours in the stress maps show very little propagation of stress radially, indicating that the bed-of-springs model of deformation, assumed in the above experimental analysis, is a good approximation. To compare average stresses from the above experimental analysis to the stresses determined from FEA calculations,  $\sigma_{zz}$  and  $\sigma_{rr}$

are integrated along the top surface of the modeled agar. We find excellent agreement between the experimental stress and  $\sigma_{zz}$ . We also find a smaller, but significant level of horizontal stress,  $\sigma_{rr}$ , which is always about 1/3  $\sigma_{zz}$ . These results demonstrate that the bed-of-springs model can be used to measure normal-stresses exerted by biofilms on their agar substrates, facilitating further study of biofilm generated forces.

## Discussion and Conclusions

Here we have shown that biofilm EPS production applies sufficient levels of stress to indent the soft, permeable, agar substrates on which colonies grow. The drag forces that occur as fluid is transported through the agar are about two orders of magnitude lower than the elastic forces associated with agar deformation. Thus, the stress generated by the biofilm can be inferred instantaneously by measuring the elastic stress exerted on the substrate surface. Geometric considerations and finite element calculations both show that the stresses are primarily normal to the surface, allowing the determination of this pressure from vertical displacement measurements.

This experimental method is analogous to traction force microscopy (TFM), a popular tool for the study of in-plane forces that tissue cells exert on soft substrates<sup>22</sup>. In contrast to TFM, the method developed here involves large displacements of a well-defined reference surface, and does not require sophisticated computational algorithms to measure displacements or to convert displacements into forces. Refinements of the method developed here, like high-resolution  $z$ -scanning, will facilitate more accurate measurements of indentation shape, which are required to reveal the physical origins of the radially varying pressure profile under the biofilm. For example, with TFM, traction forces are converted into the balancing stresses by measuring the area of contact between cell and substrate, and measuring the cell thickness. Likewise, detailed measurements of biofilm geometry and surface forces, combined with high-resolution indentation measurements may facilitate the full modelling of stresses throughout the biofilm and conditions of mechanical equilibrium. Thus, investigations of biofilm forces at higher resolution will benefit greatly from the established methods of TFM.

The role played by biofilm-produced polysaccharides in generating stress suggests that the long, flexible, polymeric sugars generate osmotic pressure, pressing the colony against

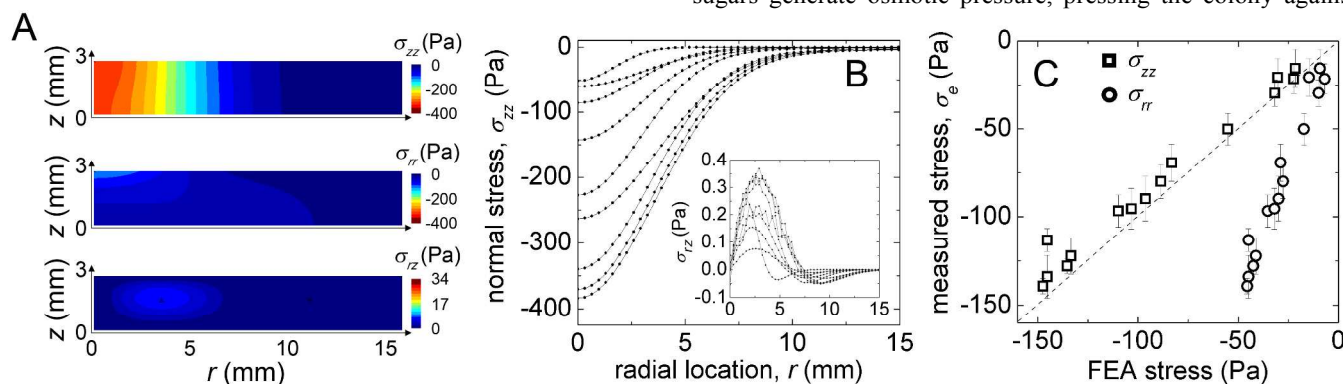


**Figure 5.** Finite element modelling of biofilm generated indentation of agar slabs. Slices through the  $r$ - $z$  plane of FEA stress maps show that the vertical component of stress,  $\sigma_{zz}$ , is consistent with a bed-of-springs approximation, while the radial and shear components of stress,  $\sigma_{rr}$  and  $\sigma_{rz}$ , are much smaller than  $\sigma_{zz}$  (A). The normal stress,  $\sigma_{zz}$ , at the surface of the agar increases and moves outward in time as the biofilm grows, while the shear stress remains about three orders of magnitude smaller than  $\sigma_{zz}$  (B). The average stress measured experimentally correlates almost perfectly with the corresponding average  $\sigma_{zz}$  from FEA calculations, and the radial stress is about 1/3  $\sigma_{zz}$  (C, dashed line denotes perfect correlation).

the agar surface as they swell and pull water across the interface. To test whether osmotic pressures generated by the EPS may be large enough to exert the stresses observed here, we employ the Van't Hoff relation describing osmotic pressure under dilute conditions,  $\Pi = k_b T N_A w^{-1} c$ , where  $\Pi$  is the osmotic pressure,  $k_b$  is Boltzmann's constant,  $T$  is the temperature,  $N_A$  is Avogadro's number,  $w$  is the polymer molecular weight, and  $c$  is the polymer concentration in units of mass per volume. For a biofilm to generate 150 Pa of pressure with polysaccharide of modest length<sup>13</sup>,  $w \sim 10^5$ , the polymer concentration within the colony would have to be  $c = 6$  mg/ml, or 0.6% by weight. The weight-percent of polysaccharides in biofilms is estimated to be of order 1%, further indicating that the stresses measured here are generated by EPS osmotic pressure. Since bacterial cells can withstand atmospheres of pressure and may stochastically fluctuate, they can bear this pressure and may also contribute to the osmotic pressure applied to the interface. In the WT biofilms, the cells constitute 10-25% of the volume fraction<sup>6, 12</sup>, suggesting that most of the osmotic pressure applied to the agar surface is due to the EPS, which has a volume fraction of 75-90%<sup>6, 12</sup>.

At early stages of growth when the colony thickens dominantly by cell proliferation, diffusion-limited nutrient depletion occurs and triggers the onset of EPS production and biofilm expansion<sup>18</sup>. With our measurements of flow into the colony, we compute a Péclet number to estimate the relative metabolic benefit from this accelerated expansion, which generates pressure driven flow of nutrient into the biofilm. The Péclet number is the ratio between the rate of advection to the rate of diffusion for a molecule to traverse a characteristic distance, given by  $Pe = \nu L D^{-1}$ , where  $\nu$  is the advection rate,  $L$  is the characteristic distance of transport, and  $D$  is the diffusivity. Since cells at the top of the biofilm will be depleted of nutrient first, we treat the characteristic length to be the thickness of the biofilm during expansion, which we previously measured to be of order 500  $\mu\text{m}$  when the biofilm is rapidly expanding and producing EPS at a high rate<sup>18</sup>. The limiting carbon source is likely to be glutamate, which has a diffusivity of  $10^{-7} \text{ cm}^2 \text{ s}^{-1}$  in water. It has been shown that diffusion is slightly slowed down in the EPS; on average the effective diffusivity of molecules in a biofilm is about  $0.4 \times D$  in water, so we estimate  $D \approx 0.4 \times 10^{-7} \text{ cm}^2 \text{ s}^{-1}$ <sup>24, 25</sup>. Using these parameters and  $\nu = 20 \mu\text{m hr}^{-1}$ , we find  $Pe \approx 0.7$ . Thus, it is possible that pressure driven flow of fluid into the colony during the rapid expansion period enhances the delivery of nutrients relative to diffusion alone. The extent to which biofilms in infected tissue or growing on cellulosic plant tissue can extract nutrients through EPS generated osmotic pressure will be explored in future work. The results presented here uncover the potential role played by the elasticity and hydraulic permeability of these materials on which biofilms grow.

## Materials and methods

*Bacillus subtilis* strain NCIB3610 is used in the work described here. Cells are kept cryogenically stored and streaked from frozen stocks onto a 1.5% agar, Luria Bertani (LB) medium plate. After 12 h of incubation at 37°C, we inoculate 3 ml of LB liquid with cells from an isolated colony. The inoculated LB medium is incubated on a shaker at 37°C for 3 h when the optical density of the bacteria solution is approximately 1. 0.5  $\mu\text{L}$  of liquid culture is spotted onto an MSgg-agar (minimal salts glycerol glutamate medium) plate or cylindrical tube for time-lapse microscopy or macro-imaging<sup>20</sup>. In control experiments, a mutant strain that is incapable of producing the

polysaccharide component of EPS is used. We refer to this strain as the eps mutant (EPS<sup>-</sup>) because the epsA-O operon encodes the polysaccharide component of the extracellular matrix<sup>21</sup>.

Error-bars in Fig. 2 A,B are the experimental uncertainty of determining the vertical location of the agar surface ( $\pm 5.5 \mu\text{m}$ ). This uncertainty is set by the low numerical aperture of the long-working distance objective needed to image through the thick agar slabs. Error-bars in Fig. 2 C,D are the combined 95% confidence interval of fitting the width and amplitude of a Gaussian function to the data. Error-bars in Fig. 3 are 95% confidence intervals for fitting the center location of a Gaussian curve to the intensity distribution in instantaneous slices of the measured kymographs. These errors are propagated to the calculations of stress shown in Fig. 4.

## Acknowledgements

We thank Hera Vlamakis, Yunrong (Win) Chai, Roberto Kolter and Richard Losick for *B. subtilis* strains used in these studies and for helpful advice and guidance.

## Notes and references

<sup>a</sup> Department of Materials Science and Engineering, University of Florida, Gainesville, FL 32611, USA.

<sup>b</sup> Department of Mechanical and Aerospace Engineering, University of Florida, Gainesville, FL 32611, USA.

<sup>c</sup> School of Engineering, University of California, Merced, CA 95343, USA.

<sup>d</sup> J. Crayton Pruitt Family Department of Biomedical Engineering, University of Florida, Gainesville, FL 32611, USA.

<sup>e</sup> Institute for Cell Engineering and Regenerative Medicine, University of Florida, Gainesville, FL 32611, USA.

1. A. G. Gristina, *Science*, 1987, 237, 1588-1595.
2. K. L. Frank, J. L. del Pozo and R. Patel, *Clinical microbiology reviews*, 2008, 21, 111-133.
3. J. Del Pozo and R. Patel, *Clinical Pharmacology & Therapeutics*, 2007, 82, 204-209.
4. P. E. Kolenbrander, *Annual Reviews in Microbiology*, 2000, 54, 413-437.
5. P. E. Kolenbrander, R. N. Andersen, D. S. Blehert, P. G. Eglund, J. S. Foster and R. J. Palmer, *Microbiology and molecular biology reviews*, 2002, 66, 486-505.
6. J. W. Costerton, K. Cheng, G. G. Geesey, T. I. Ladd, J. C. Nickel, M. Dasgupta and T. J. Marrie, *Annual Reviews in Microbiology*, 1987, 41, 435-464.
7. M. Böl, A. E. Ehret, A. Bolea Albero, J. Hellriegel and R. Krull, *Critical reviews in biotechnology*, 2013, 33, 145-171.
8. O. Galy, P. Latour-Lambert, K. Zrelli, J.-M. Ghigo, C. Beloin and N. Henry, *Biophysical journal*, 2012, 103, 1400-1408.
9. S. Tsuneda, H. Aikawa, H. Hayashi, A. Yuasa and A. Hirata, *FEMS Microbiology Letters*, 2003, 223, 287-292.
10. C. Mayer, R. Moritz, C. Kirschner, W. Borchard, R. Maibaum, J. Wingender and H.-C. Flemming, *International journal of biological macromolecules*, 1999, 26, 3-16.

## ARTICLE

11. S. S. Branda, Å. Vik, L. Friedman and R. Kolter, *Trends in microbiology*, 2005, 13, 20-26.
12. T. R. Garrett, M. Bhakoo and Z. Zhang, *Progress in Natural Science*, 2008, 18, 1049-1056.
13. H.-C. Flemming and J. Wingender, *Nature Reviews Microbiology*, 2010, 8, 623-633.
14. B. Vu, M. Chen, R. J. Crawford and E. P. Ivanova, *Molecules*, 2009, 14, 2535-2554.
15. S. Grobe, J. Wingender and H. Trüper, *Journal of applied bacteriology*, 1995, 79, 94-102.
16. I. W. Sutherland, *Microbiology*, 2001, 147, 3-9.
17. A. Seminara, T. E. Angelini, J. N. Wilking, H. Vlamakis, S. Ebrahim, R. Kolter, D. A. Weitz and M. P. Brenner, *Proceedings of the National Academy of Sciences*, 2012, 109, 1116-1121.
18. W. Zhang, A. Seminara, M. Suaris, M. P. Brenner, D. A. Weitz and T. E. Angelini, *New Journal of Physics*, 2014, 16, 015028.
19. H. Vlamakis, Y. Chai, P. Beauregard, R. Losick and R. Kolter, *Nature Reviews Microbiology*, 2013, 11, 157-168.
20. S. S. Branda, J. E. González-Pastor, S. Ben-Yehuda, R. Losick and R. Kolter, *Proceedings of the National Academy of Sciences*, 2001, 98, 11621-11626.
21. H. Vlamakis, C. Aguilar, R. Losick and R. Kolter, *Genes & development*, 2008, 22, 945-953.
22. N. Fatin-Rouge, K. J. Wilkinson and J. Buffle, *The Journal of Physical Chemistry B*, 2006, 110, 20133-20142.
23. K. Ross and M. Scanlon, *Journal of texture studies*, 1999, 30, 17-27.
24. P. S. Stewart, *Biotechnology and bioengineering*, 1998, 59, 261-272.
25. R. Schnabel, P. Langer and S. Breitenbach, *Journal of membrane science*, 1988, 36, 55-66.